Two methods for estimating limits to large-scale wind power generation

Lee M. Miller[a,1], Nathaniel A. Brunsell[b], David B. Mechem[b], Fabian Gans[a], Andrew J. Monaghan[c], Robert Vautard[d], David W. Keith[e], and Axel Kleidon[a]

[a]Max Planck Institute for Biogeochemistry, 07701 Jena, Germany; [b]University of Kansas, Lawrence, KS 66045; [c]National Center for Atmospheric Research, Boulder, CO 80305; [d]Laboratoire des Sciences du Climat et de l'Environnement, Institut Pierre-Simon Laplace, Laboratoire Commissariat à l'Énergie Atomique, CNRS, Université de Versailles Saint-Quentin-en-Yvelines, Gif/Yvette Cedex, 78000 Versailles, France; and [e]Harvard University, Cambridge, MA 02138

Edited* by Christopher J. R. Garrett, University of Victoria, Victoria, BC, Canada, and approved June 25, 2015 (received for review May 6, 2014)

Wind turbines remove kinetic energy from the atmospheric flow, which reduces wind speeds and limits generation rates of large wind farms. These interactions can be approximated using a vertical kinetic energy (VKE) flux method, which predicts that the maximum power generation potential is 26% of the instantaneous downward transport of kinetic energy using the preturbine climatology. We compare the energy flux method to the Weather Research and Forecasting (WRF) regional atmospheric model equipped with a wind turbine parameterization over a 10^5 km^2 region in the central United States. The WRF simulations yield a maximum generation of 1.1 $W_e \cdot m^{-2}$, whereas the VKE method predicts the time series while underestimating the maximum generation rate by about 50%. Because VKE derives the generation limit from the preturbine climatology, potential changes in the vertical kinetic energy flux from the free atmosphere are not considered. Such changes are important at night when WRF estimates are about twice the VKE value because wind turbines interact with the decoupled nocturnal low-level jet in this region. Daytime estimates agree better to 20% because the wind turbines induce comparatively small changes to the downward kinetic energy flux. This combination of downward transport limits and wind speed reductions explains why large-scale wind power generation in windy regions is limited to about 1 $W_e \cdot m^{-2}$, with VKE capturing this combination in a comparatively simple way.

generation limits | turbine–atmosphere interactions | wind resource | kinetic energy flux | extraction limits

Wind power has progressed from being a minor source of electricity to a technology that accounted for 3.3% of electricity generation in the United States and 2.9% globally in 2011 (1, 2). Combined with an increase in quantity, the average US wind turbine also changed from 2001 to 2012; hub height increased by 40%, rotor-swept area increased by 180%, and rated capacity increased by 100% (2). Likely a combination of both the above-noted technological innovations and improved siting, the per-turbine capacity factor, the ratio of the electricity generation rate (MW_e) to the rated capacity (MW_i), increased globally from 17% in 2001 to 29% in 2012 (1, 2), making a recently deployed wind farm likely to generate about 70% more electricity from the same installed capacity.

Combining climate datasets with these observed trends of greater-rated capacities and capacity factors, several academic and government research studies estimate large-scale wind power electricity generation rates of up to 7 $W_e \cdot m^{-2}$ (3–7). However, a growing body of research suggests that as larger wind farms cover more of the Earth's surface, the limits of atmospheric kinetic energy generation, downward transport, and extraction by wind turbines limits large-scale electricity generation rates in windy regions to about 1.0 $W_e \cdot m^{-2}$ (8–14). Ideally, these inherent atmospheric limitations to generating electricity with wind power could be considered without scenario- and technology-specific complex modeling approaches, be easily applied to "preturbine" climatologies, and yield spatially and temporally variable generation rates comparable to the energetically consistent atmospheric modeling methods.

Here, we describe such a simple method that focuses on the vertical downward transport of kinetic energy from higher regions of the atmosphere to the surface. In the absence of wind farms, the downward flux of kinetic energy is dissipated by turbulence near the surface, which shapes near-surface wind speeds. When wind farms use some of this kinetic energy, the vertical balance between the downward kinetic energy flux and turbulent dissipation is altered and results in lower hub-height wind speeds. The more kinetic energy wind farms use, the greater the shift in the balance and the reduction of wind speeds should be. This trade-off between greater utilization and lower wind speeds results in a maximum in wind power generation from the vertical flux of kinetic energy (10). This maximum yields a potential for wind power generation of a region that is independent of the technological specifications of the turbines. Because this method is based on the vertical downward transport of kinetic energy, we refer to it as the vertical kinetic energy (VKE) method. Note that this reasoning assumes that the downward flux of kinetic energy remains unchanged, which was shown to be a reasonable assumption compared with climate model simulations at the continental scale (11), but which may not hold at the regional scale.

Here we evaluate the applicability of this method by using high-resolution simulations with the Weather Research and Forecasting (WRF) regional atmospheric model with a wind turbine parameterization. We use the region of central Kansas during the typical climatological period of June–September 2001, noting that this

Significance

Wind turbines generate electricity by removing kinetic energy from the atmosphere. We show that the limited replenishment of kinetic energy from aloft limits wind power generation rates at scales sufficiently large that horizontal fluxes of kinetic energy can be ignored. We evaluate these factors with regional atmospheric model simulations and find that generation limits can be estimated from the "preturbine" climatology by comparatively simple means, working best when the atmosphere between the surface and hub height is naturally well-mixed during the day. Our results show that the reduction of wind speeds and limited downward fluxes determine the limits in large-scale wind power generation to less than 1 $W \cdot m^{-2}$.

Author contributions: L.M.M., N.A.B., and A.K. designed research; L.M.M., N.A.B., D.B.M., F.G., A.J.M., R.V., D.W.K., and A.K. performed research; L.M.M., N.A.B., D.B.M., and A.K. analyzed data; and L.M.M., N.A.B., D.B.M., A.J.M., R.V., D.W.K., and A.K. wrote the paper.

The authors declare no conflict of interest.

*This Direct Submission article had a prearranged editor.

Freely available online through the PNAS open access option.

[1]To whom correspondence should be addressed. Email: lmiller@bgc-jena.mpg.de.

This article contains supporting information online at www.pnas.org/lookup/suppl/doi:10.1073/pnas.1408251112/-/DCSupplemental.

period is before large-scale wind power deployment within this region. We then use the WRF simulation of this time period without wind farm effects to obtain the downward transport of kinetic energy into the region. This flux is used by the VKE method to predict the limit for wind power generation of the region. This limit as well as its temporal variations are then compared with a set of sensitivity simulations of the WRF model using different installed capacities of 0.3–100 $MW_i \cdot km^{-2}$ to derive the maximum wind power generation rate (the WRF method). These regional results will then be used within a broader interpretation on the role of horizontal and vertical kinetic energy fluxes to wind farms of differing installed capacities and spatial scales. We close with a brief conclusion on the implications of these two approaches for estimating large-scale wind power generation.

Methods

To evaluate the limits to wind power generation, we use a reference climatology of Central Kansas for the time period of May 15 to September 30, 2001 using the WRF-ARW v3.3.1 regional weather forecasting model (15, 16), forced with North American Regional Reanalysis data (17). This particular time period is climatologically representative for this region: a near-neutral El Niño southern oscillation phase, a climatologically standard position and strength of the Great Plains low-level jet, and an average summer soil moisture content (18). The simulation uses a single domain with a horizontal grid spacing of 12 km and 31 vertical levels, and the first 15 d of the simulation are excluded from the analysis to avoid spin-up effects. This WRF simulation represents our control simulation, which is used as input to the VKE method and as a reference for various WRF simulations with different densities of installed wind turbines to obtain the limit for wind power generation using the WRF method.

WRF Method. To estimate wind power generation using WRF, we use a version of the model that includes a parameterization of wind turbines that is slightly modified from a previously used approach (12, 19). This parameterization has been shown to be more realistic than previous roughness-based approaches (19). We perform a set of eight sensitivity simulations with different installed capacities of wind turbines that are placed within a contiguous wind farm region of 112,320 km^2 in central Kansas. Installed capacities (in units of $MW_i \cdot km^{-2}$) are simulated as an increased integrated quantity of wind turbines deployed to 780 grid cells of 144 km^2 each, which collectively represents the wind farm region. We use values of 0.3125, 0.625, 1.25, 2.5, 5.0, 10, 25, and 100 $MW_i \cdot km^{-2}$ for the installed capacities in the simulations and refer to the simulations by these capacities. The wind turbine characteristics are specified using the technical specifications of the Vestas V112 3.0 MW_i in terms of its power, thrust, and standing coefficients (see *SI Appendix* for the detailed model configuration). Note that this model setup does not have sufficient horizontal or vertical resolution to simulate interturbine interactions or wakes within the 12- × 12-km resolution grid cell, but rather uses the turbine specifications and installed capacity to derive one aggregate wind turbine for each grid cell and, where appropriate, the corresponding vertical levels. Additional simulations were performed to evaluate the sensitivity to the horizontal (to 3 km) and vertical spacing (to 24 levels in the lowest 1 km, 6 within the vertical rotor swept height) over a representative time period of June 15–21 and were found to yield comparable results (*SI Appendix*, Fig. 5).

VKE Flux Method. The VKE method expands upon one of the approaches of refs. 10 and 11, where a thought experiment illustrated how considering only wind speeds and turbine specifications can yield generation rates that are physically unrealizable. The method is based on an analytical description of the momentum balance of the wind farm, a central concept used in similar studies on large-scale wind power limits (20–22) or for other forms of renewable energy such as tidal power (23, 24) (detailed methodology is given in *SI Appendix*). It assumes that when wind farms extend tens of kilometers downwind, horizontal kinetic energy has either been extracted from the mean flow by the first few rows of turbines or has been lost to turbulent dissipation, so that the generation rate of wind turbines further downwind is then limited by the downward flux of kinetic energy. For this reason, it is assumed that the horizontal kinetic energy flux can be neglected for large-scale wind farms, allowing us to estimate the maximum extraction rate of kinetic energy by the turbines from the vertical downward flux of kinetic energy from the atmosphere above the wind farm. The model yields an analytic expression for the maximum extraction rate, $P_{max} = (2\sqrt{3}/9) \cdot \rho u_*^2 \cdot v_0$, where ρ is the air density, u_* is the friction velocity at the surface, and v_0 is the wind speed of the control simulation at the 84-m hub height. Note that in addition to the wind speed (v_0), this method uses the surface friction velocity (u_*) as an additional meteorological variable to yield the rate P_{max}. This additional information is not used in common methods that evaluate limits to wind power generation using only wind speeds and a prescribed installed capacity (3–7). We then convert this maximum rate into a limit for electricity generation by using the Betz limit and estimates of wake turbulence (25), resulting in a reduction to about 66%, or two-thirds, of P_{max}. Thus, we define the maximum electricity generation rate by a large wind farm as $P_e = (4\sqrt{3}/27) \cdot \rho u_*^2 \cdot v_0$. This results in the maximum electricity generation rate, P_e, to be equivalent to $(4\sqrt{3}/27) = 26\%$ of the turbulent dissipation occurring before wind farm deployment. Note that P_e is not specific to an installed capacity or wind turbine manufacturer specifications, thereby resulting in the maximum wind power generation rate possible from the pre-turbine climatological vertical kinetic energy flux through hub height.

Results and Discussion

As shown in Fig. 1, the WRF simulations show that a greater installed capacity within the wind farm region increases the total electricity generation rate. This increase is almost linear at the lower installed capacities (0.3 $MW_i \cdot km^{-2} \approx 0.13$ $W_e \cdot m^{-2}$, 0.6 $MW_i \cdot km^{-2} \approx 0.24$ $W_e \cdot m^{-2}$; subscripts i and e refer to the installed capacity and electricity generation, respectively). With further increases in the installed capacity, the marginal return of electricity generation predominantly occurs during higher wind speed periods. Such greater generation rates during windy periods can be seen in the differences between the simulations with 5.0 and 10 $MW_i \cdot km^{-2}$ during the high wind speeds of June, whereas the difference is smaller during the lower wind speeds of August and September. Because the greater generation rates occur during periods that are less frequent, the increase in generation is no longer linear. This is reflected by comparing the generated electricity of the 5.0 $MW_i \cdot km^{-2}$ to the 0.3 $MW_i \cdot km^{-2}$ simulation, which generates seven times more electricity with 16 times as many wind turbines. Stated differently, each wind turbine at 5.0 $MW_i \cdot km^{-2}$ generates electricity at half the rate as wind turbines with the same technical specifications but installed at 0.3 $MW_i \cdot km^{-2}$.

This difference in the relationship between generation rate and installed capacity is reflected in a change in the capacity factor. First, we use the hub-height wind speeds of the control simulation and the turbine power curve for the Vestas V112 turbine (*SI Appendix*, Fig. 6) to calculate the generation rate of a single isolated wind turbine deployed to each location and time. This yields a capacity factor of 47%, which represents the upper bound value for the case of no interactions between the wind turbines and the atmospheric flow. This estimate compares well to the capacity factors of 22–36% (1, 7) derived from installed capacity and operational generation data from Kansas during 2006–2012, even though this estimate includes turbines of various technical specifications taken over a much longer timescale than this study. Using the 2012 installed capacity of 2,713 MW_i (7) and the area of 213,000 km^2 for Kansas yields a state-scale installed capacity of

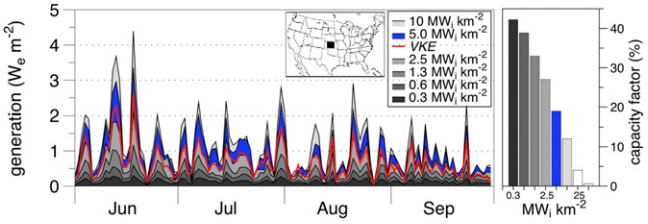

Fig. 1. (*Left*) Simulated daily mean electricity generation rates over the Kansas wind farm region (black square on map) for different installed capacities of up to 10 $MW_i \cdot km^{-2}$. The higher installed capacities of 25 and 100 $MW_i \cdot km^{-2}$ are not shown, because they often yield less than the 10 $MW_i \cdot km^{-2}$ simulation. For comparison, the VKE estimate is shown in red. (*Right*) The mean per-turbine capacity factor derived for the different simulations.

0.013 $MW_i \cdot km^{-2}$, which falls below the lowest installed capacity that we used. Our simulation with the lowest installed capacity of 0.3 $MW_i \cdot km^{-2}$ corresponds to a slightly reduced capacity factor of 42%, and 39% with 0.6 $MW_i \cdot km^{-2}$ (*SI Appendix*, Table 2). These capacity factors compare well with the previously used values for this region of 37% (6) and 40–47% used by the National Renewable Energy Laboratory (7). However, the estimates of refs. 6 and 7 used an installed capacity of 5.0 $MW_i \cdot km^{-2}$, which in our simulations yield a much lower capacity factor of 19%, which should thus result in much lower estimates for wind power generation.

The reduction in capacity factor with greater installed capacity results from an enhanced interaction of wind turbines with the atmospheric flow. Because a greater installed capacity of wind turbines removes more kinetic energy from the atmosphere and converts it into electric energy, this causes a decrease in the hub-height wind speed downwind (26), which decreases the mean per-turbine electricity generation rate of the wind farm. This reduction in wind speeds within the wind farm and its effects on the per-turbine electricity generation rate is shown in Fig. 2 in relation to the power curve of the turbine and the wind speed histogram (Fig. 2*A*) as well as the mean wind speed and mean per-turbine generation rate (Fig. 2*B*). The point spread around the 3.0 MW_i turbine power curve in Fig. 2*A*, with some values below the 3.0 $m \cdot s^{-1}$ cut-in wind speed, is due to the use of mean hourly hub-height wind speed and electricity generation rate for the entire wind farm region. Additionally, the variability in hub-height wind speed decreases with greater installed capacity (Fig. 2*B*), which also decreases the variability of per-turbine electricity generation. This reduction in wind speeds has also been observed in previous modeling studies (9–12, 27, 28).

Fig. 2*C* shows the increasing importance of considering the reduction in wind speed for the mean generation rate of the wind farm with greater installed capacity. The dashed line in Fig. 2*C* is derived by applying the turbine power curve to the control hub-height wind speeds for a mean per-turbine capacity factor of 47% (slope = 0.47). The WRF simulations with installed capacities of less than about 1 $MW_i \cdot km^{-2}$ yield similar estimates because the capacity factors remain high (see also *SI Appendix*, Table 2). At greater installed capacities, the WRF simulations resulted in proportionally lower estimates. For example, at an installed capacity of 2.5 $MW_i \cdot km^{-2}$ the "no interactions" estimate would yield a generation rate per unit area of the wind farm of 1.18 $W_e \cdot m^{-2}$, but this was simulated to be 0.68 $W_e \cdot m^{-2}$. This discrepancy continues with greater installed capacities, so at 5.0 $MW_i \cdot km^{-2}$ the estimate without interactions overestimates the average electricity generation rate by more than a factor of two (2.4 $W_e \cdot m^{-2}$ for no interactions, 0.95 $W_e \cdot m^{-2}$ with interactions). The maximum electricity generation rate of 1.1 $W_e \cdot m^{-2}$ is obtained with an installed capacity of 10 $MW_i \cdot km^{-2}$, at which the associated hub-height wind speed decreased by 42% and the capacity factor is reduced to 12%. Our WRF simulations suggest that previous estimates of mean wind energy generation potentials for Kansas of 1.9 $W_e \cdot m^{-2}$ (6), 2.0–2.4 $W_e \cdot m^{-2}$ (7), and 2.5 $W_e \cdot m^{-2}$ (4) are likely to be too high because the effects of reduced wind speeds were not considered. To place this reduction into the context of present-day wind power deployment, note that such installed capacities are several orders of magnitude larger than presently operational Kansas wind farms. Our simulations thus suggest that an equidistant deployment of 50 times more installed wind power in Kansas than is presently operational ($\approx$ 0.013–0.6 $MW_i \cdot km^{-2}$) would maintain the presently high per-turbine capacity factors and thus increase the generation rate 50-fold.

The VKE method captures the magnitude of wind power generation as well as its temporal variations. In our Kansas scenario, we estimate a maximum 4-mo mean generation rate from WRF at 10 $MW_i \cdot km^{-2}$ as 1.1 $W_e \cdot m^{-2}$ and VKE as 0.64 $W_e \cdot m^{-2}$. Based on the linear correlation, the daily mean estimates of the two methods are highly correlated: $r^2 = 0.98$, with a slope of $m = 1.76$, an rmse of 0.60, and a mean absolute error (MAE) of 0.47. The WRF estimate from the 5.0 $MW_i \cdot km^{-2}$ simulation, an installed capacity often used for wind power planning and policy analysis (6), also compares very well, with daily mean estimates being highly correlated with VKE with $r^2 = 0.98$, $m = 1.47$, rmse = 0.39, and MAE = 0.32. The mean generation rate of this WRF simulation was 0.95 $W_e \cdot m^{-2}$, nearly the same rate as the 10 $MW_i \cdot km^{-2}$ simulation, but from half the number of turbines. When hourly estimates of WRF and VKE are compared (Fig. 3), we note that correlations are very high during day and night, but the slope is much better captured by VKE during the day, whereas at night VKE underestimates the magnitude of electricity generation by almost 45% in this simulation.

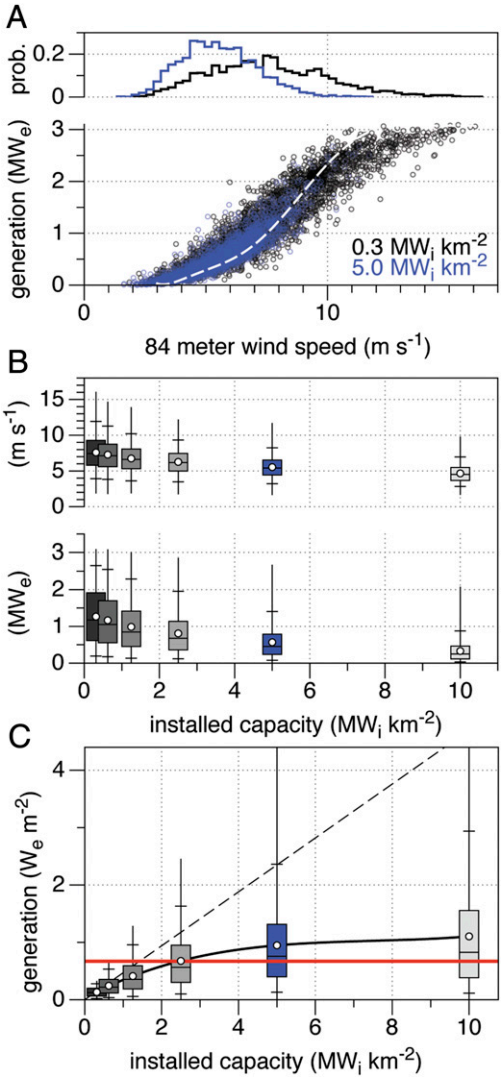

Fig. 2. (*A*) The per-turbine electricity generation rate for two select WRF simulations as a function of hub-height wind speed at 84 m as well as its histogram (*Top*). The dashed line shows the Vestas V112 3.0 MW_i power curve of a single turbine. (*B*) Mean per-turbine generation rate and the 84 m mean hub-height wind speed of the wind farm region as a function of installed capacity. (*C*) Mean per-turbine electricity generation rate as a function of installed capacity when the capacity factor of a single turbine is extrapolated to high installed capacities (dashed line, "no interactions") and the relationship derived from the WRF simulations (solid line, "interactions"). The red line shows the VKE estimate. All box-whisker plots show the 5, 25, 50, 75, and 95% values, with the extent showing the minimum–maximum and the circles showing the mean.

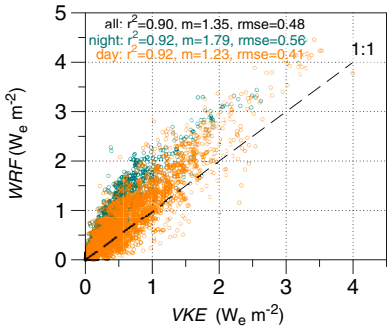

Fig. 3. Comparison of hourly mean electricity generation rates for the wind farm region estimated by VKE and WRF with an installed capacity of 5 $MW_i \cdot km^{-2}$.

We attribute this underestimation of wind power generation by VKE at night to its use of the preturbine downward kinetic energy flux of the control. The atmospheric flow in this region typically decouples from the stable surface conditions at night in the summer, which leads to the formation of the low-level jet (LLJ) near the surface (29). The typical nighttime structure of the LLJ (Fig. 4*B*) with a mean stable boundary layer height of 40 m (12–124 m, 5th–95th percentile, respectively) from June–September 2001 in the WRF control mean is consistent with height observations of about 50–350 m in southeastern Kansas during October 1999 (30). Observed LLJ maxima at about 100 m after sunset with an increase in height to about 225 m over the course of the night were also observed for this region on October 25, 1999 (30). The rotors of the wind turbines extend from 28 to 140 m in height and thus reside above, within, or at the upper boundary of the stable boundary layer. The wind turbines in the WRF simulations can thus sometimes directly use the kinetic energy from above the constant stress layer and the LLJ at night. This increased utilization of kinetic energy of the LLJ and the flow of the free atmosphere results in an increased downward kinetic energy and thus a greater maximum generation rate in WRF compared with the VKE method, which does not account for this effect. Based on the nighttime hourly mean values for the wind farm region, a hub-height speed of 9.5 $m \cdot s^{-1}$ and a surface momentum flux of 0.15 $kg \cdot m^{-1} \cdot s^{-2}$ yields a downward kinetic energy flux of 1.39 $W \cdot m^{-2}$ with an associated maximum generation rate of 0.36 $W_e \cdot m^{-2}$ by VKE. Daytime atmospheric conditions are different. The daytime mean convective boundary layer height in the WRF control simulation is 1,268 m. Of this total height, the constant stress layer, the vertical depth over which the downward kinetic energy flux is considered negligible, typically constitutes the lowest 10% of the convective boundary layer (31, 32). Therefore, during the daytime, the upper extent of the turbine rotors is likely to be within the constant stress layer. Based on mean daytime values, a hub-height speed of 6.9 $m \cdot s^{-1}$ and a surface momentum flux of 0.37 $kg \cdot m^{-1} \cdot s^{-2}$ yields a downward kinetic energy flux of 2.55 $W \cdot m^{-2}$ with an associated maximum generation rate of 0.65 $W_e \cdot m^{-2}$ by VKE. Note how the daytime VKE estimate is about double the nighttime estimate, even though the wind speed during the daytime is lower. These differences between the nighttime and daytime downward kinetic energy fluxes also help explain the similarities and discrepancies between the daytime and nighttime VKE and WRF estimates (Fig. 3).

One last point to note is that the maximum mean electricity generation rate of 1.1 $W_e \cdot m^{-2}$ achieved in WRF has notable effects on the atmosphere and would likely induce considerable differences in climate. Although several recent studies evaluated how wind power generation caused climatic differences in measurements (33, 34) and modeling (10, 12, 13, 27, 35–37), the reduction of wind speeds is relevant here, because this reduction sets the large-scale limit to wind power generation. The mean hub-height wind speed in the 10 $MW_i \cdot km^{-2}$ decreased by 42% compared with the control (Fig. 2*B*). This decrease is consistent with VKE, which provides an analytic expression for the decrease in wind speed at maximum generation of $(1-\sqrt{3}/3)\cdot v_0 = 42\%$. As described above, it is this decrease in wind speed with greater kinetic energy extraction by more wind turbines that limits the wind power generation at large scales. That VKE reproduces the decrease in v_0 very well is likely the reason why it captures the magnitude and temporal dynamics of limits to large-scale wind power generation of the WRF simulation.

Interpretation

Our estimates from both methods are compared with several other recent studies in Fig. 5. There is a clear discrepancy between estimates based on climatological wind speeds (black symbols) from estimates derived with atmospheric models (colored symbols), which are generally lower. We attribute these discrepancies to the inclusion of turbine–atmosphere interactions in the case of the atmospheric models that result in the reduction of wind speeds in the wind farm. However, one study included in Fig. 5 was derived from existing operational wind farms and observed generation rates, which calls for a more detailed explanation of the discrepancy between those and our estimates. Numerous footprints of operational wind farms in the United Kingdom were digitized (38) and compared with their documented generation rate, thereby inherently including turbine–atmosphere interactions. With the majority of the wind farms used in ref. 38 covering relatively small areas of about 2.4 km^2 (0.1–13 km^2) of "footprint area" in hilltop or offshore locations, the wind farms have a mean generation rate of about

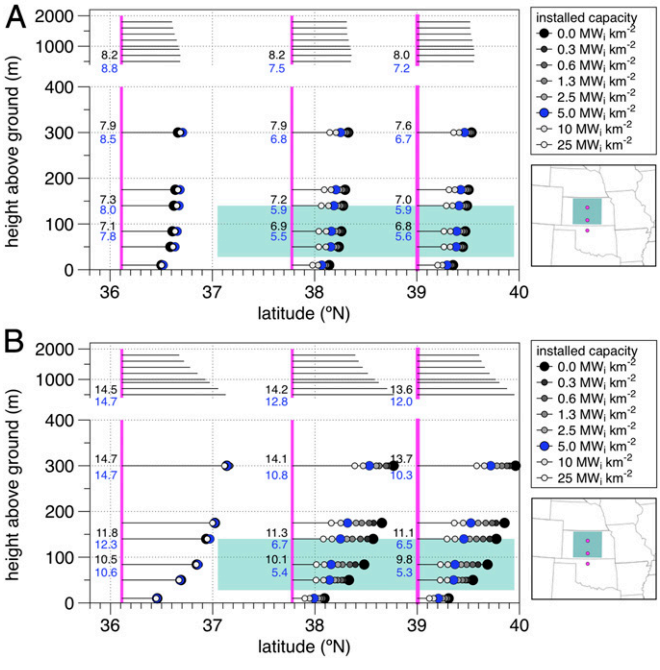

Fig. 4. Mean (*A*) daytime and (*B*) nighttime wind speeds for three selected locations across the wind farm region (*Inset*) for the control and seven WRF simulations with different installed capacities with one location generally upwind and two locations within the wind farm region. The teal boxes show the spatial and vertical extent of the wind farm. The pink bars and dots show the spatial locations where the mean wind speeds were taken. Wind speeds at the hub height of 84 m and top-of-rotor height of 140, 300, and 500 m for the three locations are noted as text for the control (black numbers) and 5.0 $MW_i \cdot km^{-2}$ (blue numbers). Note the break in both *y* axes.

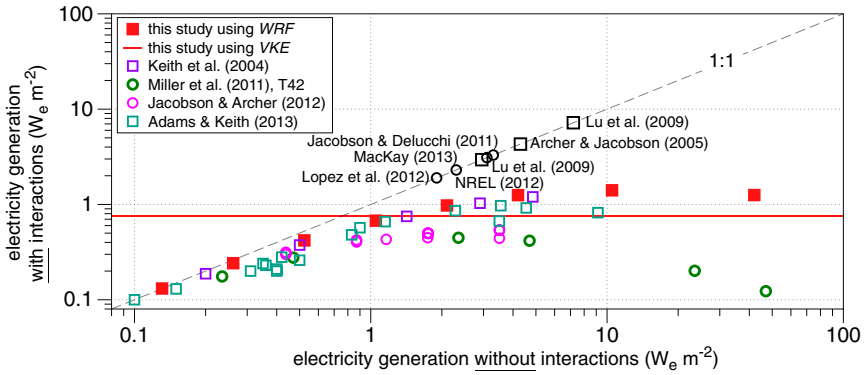

Fig. 5. Regional (squares) and continental-to global scale (circles) large-scale electricity generation estimates in relation to the effect of turbine–atmosphere interactions. The estimates represented by black squares and circles used preturbine wind speeds without including turbine–atmosphere interactions and are placed on the 1:1 line for reference. The colored points refer to estimates based on atmospheric models. These estimates simulate wind speeds and include turbine–atmosphere interactions (*y* axis). The value on the x axis was derived from using the turbine power curve, installed capacity, and the wind speeds of the control simulation. The horizontal line at 0.64 $W_e{\cdot}m^2$ with interactions is the VKE estimate for Kansas (based on figure 4 from ref. 12 with additional studies and the VKE estimate added).

2.9 $W_e{\cdot}m^{-2}$ (0.8–6.6 $W_e{\cdot}m^{-2}$) from a mean installed capacity of about 11 $MW_i{\cdot}km^{-2}$ (3.5–24 $MW_i{\cdot}km^{-2}$). These generation rates are substantially higher than our 1.1 $W{\cdot}m^{-2}$ limit of large-scale wind power generation in Kansas, although the size of the wind farms is also notably smaller.

This difference in wind power generation rates can be understood by relating the kinetic energy used by the wind turbines to their sources. For this, we distinguish between the import of kinetic energy by horizontal and vertical fluxes into the wind farm region. These two contributions change as the spatial scale of the wind farm increases. This change can be illustrated by using the mean values of the wind farm region from the WRF control simulation over the 4-mo period. The mean horizontal flux of kinetic energy is given by $KE_{in,h} = (1/2)\rho v_0^3 \cdot x \cdot h$, where $\rho = 1.1$ $kg{\cdot}m^{-3}$ is the air density at hub height, $v_0 = 8.0$ $m{\cdot}s^{-1}$ is the hub-height wind speed at 84 m, $x = 360{,}000$ m is the east–west extent of the wind farm that is perpendicular to the mean wind direction, and $h = 112$ m is the height of the wind farm, assumed here to be equivalent to the rotor diameter of the 3.0 MW_i turbine. This yields a mean horizontal kinetic energy flux of $KE_{in,h} = 11$ GW (or 282 $W{\cdot}m^{-2}$ per unit cross-sectional area) into the upwind vertical cross-section of the wind farm region. The mean vertical kinetic energy flux is given by $KE_{in,v} = \rho u_*^2 \cdot v_0 \cdot x \cdot y$, where the mean (spatial and temporal) friction velocity at the surface $u_* = 0.45$ $m{\cdot}s^{-1}$ and $y = 312{,}000$ m is the north–south extent of the wind farm that describes the downwind length of the wind farm. This yields a mean vertical kinetic energy flux downward into the entire wind farm region of $KE_{in,v} = 200$ GW or 1.8 $W{\cdot}m^{-2}$ per unit surface area of the wind farm region, so that in the Kansas setup, $KE_{in,v}$ provides about 20 times as much kinetic energy as the horizontal influx. Note that this vertical flux of kinetic energy, derived from the WRF control simulation, served as the input to the VKE estimate. When the wind farm increases in downwind length with a greater value of *y*, the contribution by the vertical kinetic energy flux into the wind farm region increases linearly whereas the horizontal contribution remains relatively unchanged. WRF simulations with an installed capacity of 1 $MW_i{\cdot}km^{-2}$ or greater (>110 GW_i) represent wind farms in which the installed capacity is of the order of the mean kinetic energy flux into the wind farm region (about 211 GW), which is when the reductions of wind speed start to play a role in shaping the generation rate.

In the context of the Kansas wind farm region, we can use these considerations to estimate the downwind depth at which the horizontal kinetic energy flux is fully consumed by electricity generation and turbulence. Assuming a conservative 33% loss to turbulence during the extraction process (25), the 11-GW mean horizontal kinetic energy flux would result in a maximum electricity generation rate of 7.4 GW_e. This generation rate is equivalent to about 5,800 wind turbines of 3.0 MW_i capacity with a 42% capacity factor, which is close to our WRF simulation at the lowest installed capacity of 0.3 $MW_i{\cdot}km^{-2}$. When considering the much greater installed capacity of 5.0 $MW_i{\cdot}km^{-2}$, the 11 GW of horizontal kinetic energy flux would be fully consumed within a downwind depth of about 10 km (see also ref. 22). Therefore, as the downwind extent of the wind farm grows, electricity generation rates of successive downwind turbines are derived progressively less from the horizontal flux and more from the vertical flux. This results in an edge effect of higher generation rates at the upwind border of the wind farm compared with lower generation rates in the interior of the wind farm region (see also *SI Appendix*, Fig. 9). This edge effect does not exist for the VKE estimate (*SI Appendix*, Fig. 9), because it neglects the horizontal kinetic energy flux as an energy source. This can in part explain the lower estimates of the VKE method. However, when considering wind farms of greater sizes, the influence of this edge effect on the mean generation rate becomes progressively less important to consider.

Generation rates above those estimated by VKE could be achieved if the incoming horizontal kinetic energy flux is available to the wind farm because it was not extracted by upwind turbines, or relate to an increase in the vertical kinetic energy flux by the wind turbines, as shown to particularly occur in the WRF simulations at night. The spatial extent over which this enhanced vertical kinetic energy flux can be maintained, how much it alters the LLJ, and possibly how this results in a regional redistribution in this flux remain as open questions.

An overall increase in the downward kinetic energy flux at larger deployment scales seems unlikely to occur, because climate model simulations performed at continental and global scales do not predict such an increase for present-day radiative forcing conditions (10, 13). Although these studies did not include a full analysis of the energetics, their predictions broadly agree with the predictions of the VKE method in terms of a maximum of 25–27% of the natural dissipation rate that could be used for electricity generation (10) and a slowdown of hub-height wind velocities by 51% globally, 50% over land, and 51% over the ocean (13). Despite its lack of considering changes in the downward kinetic energy flux, it would nevertheless seem that the VKE method is suitable to provide first-order estimates of the magnitude of wind power generation by large wind farms, but this would require further confirmation.

This agreement does not resolve the apparent discrepancy between our estimates and the observation-based estimates from small UK wind farms (38); note that these wind farms have downwind depths much less than 10 km, making their electricity generation rates almost exclusively dependent on the horizontal kinetic energy flux. Formulated differently, edge effects determine the generation rate of these small wind farms. To illustrate compatibility with WRF-simulated results, we apply the footprint area definition of ref. 38 for isolated 3.0 MW_i wind turbines (i.e., a circle with diameter five times the turbine diameter, or 0.25 km^2 per turbine) to our simulation of 0.3 $MW_i{\cdot}km^{-2}$. This results in each 3.0 MW_i turbine being spaced 3.1 km apart and yields a comparable

5.1 $W_e \cdot m^{-2}$ for the turbines. For progressively larger installed capacities, this estimate decreases to 4.7 $W_e \cdot m^{-2}$ for an installed capacity of 0.6 $MW_i \cdot km^{-2}$, to 4.0 $W_e \cdot m^{-2}$ for 1.3 $MW_i \cdot km^{-2}$, to 3.3 $W_e \cdot m^{-2}$ for 2.5 $MW_i \cdot km^{-2}$, to 2.3 $W_e \cdot m^{-2}$ for 5.0 $MW_i \cdot km^{-2}$, and to 1.3 $W_e \cdot m^{-2}$ for 10 $MW_i \cdot km^{-2}$.

In summary, these considerations illustrate the strong dependence of small-scale wind farms on a horizontal kinetic energy flux that is not influenced by other wind farms upwind. Our results suggest that expanding wind farms to large scales will limit generation rates by the vertical kinetic energy flux, thereby constraining mean large-scale generation rates to about 1 $W_e \cdot m^{-2}$ even in windy regions. Large-scale estimates that exceed 1 $W_e \cdot m^{-2}$ thus seem to be inconsistent with the physical limits of kinetic energy generation and transport within the Earth's atmosphere.

Conclusion

We evaluated large-scale limits to wind power generation in a hypothetical scenario of a large wind farm in Kansas using two distinct methods. We first used the WRF regional atmospheric model in which the wind farm interacts with the atmospheric flow to derive the maximum wind power generation rate of about 1.1 $W_e \cdot m^{-2}$. This maximum rate results from a trade-off by which a greater installed capacity resulted in a greater reduction of wind speeds within the wind farm. This reduction in wind speeds reflects the strong interaction of the wind farm with the atmospheric flow, with speeds reduced by 42% at the maximum generation rate. We then showed that these estimates can also be derived by the VKE method, which used the downward influx of kinetic energy of the control climatology and its partitioning into turbulent dissipation and wind-energy generation as a basis. The VKE method predicts that the maximum generation rate equals 26% of the instantaneous downward transport of kinetic energy through hub height. This method only required the information of wind speeds and friction velocity of the control climate to provide an estimate of a maximum wind power generation rate. With an estimate of 0.64 $W_e \cdot m^{-2}$, the VKE method underestimates the maximum wind power generation rate, particularly during night, but it nevertheless captures the temporal dynamics as well as the reduction in wind speeds very well.

Both methods used here yield estimates for the limits to large-scale wind power generation that are energetically consistent. Although many current wind farms are still comparatively small and can therefore sustain greater generation rates, an energetically consistent approach becomes relevant when the installed capacity of the wind farm approaches the kinetic energy flux into the wind farm region. Although the VKE method assumes this influx to be fixed, it nevertheless demonstrates that an energetically consistent estimate can be done in a comparatively simple way, thus providing a useful means to derive a first-order estimate of large-scale wind power generation from preturbine climatologies. We conclude that large-scale wind power generation is thus limited to a maximum of about 1 $W_e \cdot m^{-2}$ because of this inevitable reduction of wind speeds and the comparatively low vertical kinetic energy fluxes in the atmosphere.

ACKNOWLEDGMENTS. We thank C. Dhara, M. Renner, N. Carvalhais, two anonymous reviewers, and the editor for their suggestions and constructive comments that helped improve the mansucript. This study was funded by the Max Planck Society through the Max Planck Research Group of A.K. A.J.M. was funded by the National Science Foundation.

1. US Energy Information Administration (2014) Annual energy review. Available at www.eia.gov/totalenergy/data/monthly/. Accessed July 28, 2015.
2. Wiser R, Bolinger M (2012) 2011 Wind technologies market report.US Department of Energy, Energy Efficiency & Renewable Energy report DOE/GO-102012-3472 (US Department of Energy, Oak Ridge, TN).
3. Archer C, Jacobson M (2005) Evaluation of global wind power. *J Geophys Res* 110(D12):D12110.
4. Lu X, McElroy MB, Kiviluoma J (2009) Global potential for wind-generated electricity. *Proc Natl Acad Sci USA* 106(27):10933–10938.
5. Jacobson MZ, Delucchi M (2011) Providing all global energy with wind, water, and solar power, Part I: Technologies, energy resources, quantities and areas of infrastructure, and materials. *Energy Policy* 39:1154–1169.
6. Lopez A, Roberts B, Heimiller D, Blair N, Porro G (2012) U.S. renewable energy technical potentials: A GIS-based analysis. US Department of Energy National Renewable Energy Laboratory report TP-6A20-51946 (US Department of Energy, Golden, CO).
7. National Renewable Energy Laboratory (2012) Stakeholder engagement and outreach. Available at apps2.eere.energy.gov/wind/windexchange/pdfs/wind_maps/wind_potential.pdf and apps2.eere.energy.gov/wind/windexchange/wind_installed_capacity.asp. Accessed May 2, 2014.
8. Gustavson MR (1979) Limits to wind power utilization. *Science* 204(4388):13–17.
9. Keith DW, et al. (2004) The influence of large-scale wind power on global climate. *Proc Natl Acad Sci USA* 101(46):16115–16120.
10. Miller LM, Gans F, Kleidon A (2011) Estimating maximum global land surface wind power extractability and associated climatic consequences. *Earth Syst. Dynam* 2:1–12.
11. Gans F, Miller LM, Kleidon A (2012) The problem of the second wind turbine — a note on common but flawed wind power estimation methods. *Earth Syst. Dynam* 3:79–86.
12. Adams AS, Keith D (2013) Are global wind power resource estimates overstated? *Environ Res Lett* 8:015021.
13. Jacobson MZ, Archer CL (2012) Saturation wind power potential and its implications for wind energy. *Proc Natl Acad Sci USA* 109(39):15679–15684.
14. Kirk-Davidoff D (2013) Plenty of wind. *Nat Clim Chang* 3:99–100.
15. Skamarock WC, et al. (2008) A description of the advanced research WRF version 3. NCAR technical note NCAR/TN-475+STR (National Center for Atmospheric Research, Boulder, CO).
16. Wang W, et al. (2012) *WRF ARW V3: User's Guide* (National Center for Atmospheric Research, Boulder, CO).
17. Mesinger F, et al. (2006) North American Regional Reanalysis. *Bull Am Meteorol Soc* 87:343–360.
18. Trier S, Davis C, Ahijevych D (2009) Environmental controls on the simulated diurnal cycle of warm-season precipitation in the continental United States. *J Atmos Sci* 67: 1066–1090.
19. Fitch A, Olson J, Lundquist J (2013) Parameterization of wind farms in climate models. *J Clim* 26:6439–6458.
20. Calaf M, Meneveau C, Meyers J (2010) Large eddy simulation study of fully developed wind-turbine array boundary layers. *Phys Fluids* 22:015110-1–015110-16.
21. Meyers J, Meneveau C (2012) Optimal turbine spacing in fully developed wind farm boundary layers. *Wind Energ.* 15:305–317.
22. Meneveau C (2012) The top-down model of wind farm boundary layers and its applications. *J Turbul* 13:1–12.
23. Garrett C, Cummins P (2007) The efficiency of a turbine in a tidal channel. *J Fluid Mech* 588:243–251.
24. Garrett C, Cummins P (2013) Maximum power from a turbine farm in shallow water. *J Fluid Mech* 714:634–643.
25. Corten G (2001) Novel views on the extraction of energy from wind: Heat generation and terrain concentration. Proceedings of the 2001 EWEC conference. Available at www.ecn.nl/docs/library/report/2001/rx01054.pdf. Accessed May 2, 2014.
26. Iungo G, Wu Y, Porté-Agel F (2013) Field measurements of wind turbine wakes with lidars. *J Atmos Ocean Technol* 30:274–287.
27. Miller LM, Gans F, Kleidon A (2011) Jet stream wind power as a renewable energy resource: Little power, big impacts. *Earth Syst. Dynam* 2:201–212.
28. Fitch A, et al. (2012) Local and mesoscale impacts of wind farms as parameterized in a mesoscale NWP model. *Mon Weather Rev* 140:3017–3038.
29. Blackadar A (1957) Boundary layer wind maxima and their significance for the growth of nocturnal inversions. *Bull Am Meteorol Soc* 38(5):283–290.
30. Pichugina Y, Banta R (2009) Stable boundary layer depth from high-resolution measurements of the mean wind profile. *J Appl Meteorol Climatol* 49:20–35.
31. Driedonks A, Tennekes H (1984) Entrainment effects in the well-mixed atmospheric boundary layer. *Boundary-Layer Meteorol* 30(1-4):75–105.
32. Stull R (1988) *An Introduction to Boundary Layer Meteorology* (Springer, Berlin), Vol 13.
33. Baidya Roy S, Traiteur JJ (2010) Impacts of wind farms on surface air temperatures. *Proc Natl Acad Sci USA* 107(42):17899–17904.
34. Zhou L, et al. (2012) Impacts of wind farms on land surface temperatures. *Nat Clim Chang* 2:539–543.
35. Kirk-Davidoff D, Keith D (2008) On the climate impact of surface roughness anomalies. *J Atmos Sci* 65:2215–2234.
36. Fiedler B, Bukovsky M (2011) The effect of a giant wind farm on precipitation in a regional climate model. *Environ Res Lett* 6:045101.
37. Vautard R, et al. (2014) Regional climate model simulations indicate limited climatic impacts by operational and planned European wind farms. *Nat Commun* 5:3196.
38. MacKay DJ (2013) Could energy-intensive industries be powered by carbon-free electricity? *Philos Trans A Math Phys Eng Sci* 371(1986):20110560.

Two methods for estimating limits to large-scale wind power generation

Lee M. Miller[1], Nathaniel A. Brunsell[2], David B. Mechem[2], Fabian Gans[1], Andrew J. Monaghan[3], Robert Vautard[4], David W. Keith[5] and Axel Kleidon[1]

[1]Max-Planck Institute for Biogeochemistry, Jena (Germany)
[2]University of Kansas, Lawrence, KS (USA)
[3]National Center for Atmospheric Research, Boulder, CO (USA)
[4]LSCE/IPSL, Laboratoire CEA/CNRS/UVSQ, Gif/Yvette Cedex (France)
[5]Harvard University, Cambridge, MA (USA)

June 5, 2015

1 Model Setup

The simulations were performed with version 3.3.1 of the Advanced Research Weather Research and Forecasting model (WRF; [16]). All simulations were forced with North American Regional Reanalysis (NARR) data [13] from May 15 to September 30, 2001. The NARR forcing data was preprocessed for input into WRF using the WRF Preprocessing System (WPS). May output was excluded due to possible spin-up effects related to the turbine-atmosphere interactions directly attributed to the wind turbines.

2 WRF Method (*WRF*)

We use WRF v.3.3.1 with the Fitch et al. [7] wind power parameterization and NARR forcing data for simulating installed wind farm capacities ranging from 0.3125 to 100.0 MW_i km^{-2} within the Kansas wind farm region, where subset $_i$ signifies the installed capacity (see also Table 2). A few specific code changes were necessary to accomplish this. First, the Fitch et al. [7] wind power parameterization does not simulate the electricity generation rate of wind turbines, but rather the resulting effect of the wind turbines to the atmospheric flow. Most of the framework for introducing the calculation of electricity generation by wind turbines is already present within the WRF v.3.3.1 Fitch et al. [7] parameterization. It was necessary to incorporate

wind turbine power curves, related technical specifications to those turbines, and more fully account for the estimate of power within the Fitch et al. [7] parameterization as follows.

The Vestas V112 3.0 MW_i wind turbine was introduced into this wind power parameterization. The manufacturer's specifications were downloaded from the Technical University of Denmark (`http://www.wasp.dk/Download/Power-curves/VestasPowerCurves`). Generation rates and turbine thrust coefficients are available from 0.95 - 1.275 kg m^{-3} and at 0.5 m s^{-1} intervals between the cut-in speed of 3.0 m s^{-1} and cut-out speed of 25.0 m s^{-1}. Note that while identified as a 3.0 MW_i turbine, the Vestas V112 is capable of generating 3 075 000 watts at hub-height velocities greater than approximately 11.5 m s^{-1}.

Based on the control simulation, the mean air density within the Kansas wind farm region from June 1 - Sept. 30, 2001 was quantified as 1.11 kg m^{-3}. Therefore, the manufacturer specifications for the generation rate and thrust coefficients specific to 1.1 - 1.125 kg m^{-3} were used. The turbine power coefficient, which is also necessary to include within the Fitch et al. (2012) wind power parameterization, was derived from this generation rate curve as: power coefficient $= \frac{G}{0.5 \cdot \rho v^3 \cdot A_{rotor}}$, where G is the generation rate at the specified speed, ρ is the air density of 1.1 kg m^{-3} and A_{rotor} is the rotor swept area of 9852 m^2 (Fig. 1). At time periods and/or locations where the wind speed influencing the turbine rotors would be less than 3.0 m s^{-1} or greater than 25.0 m s^{-1}, a standing thrust coefficient of 0.049 m^{-1} was included, also based on the manufacturer specifications for this 1.1 - 1.125 kg m^{-3} air density range.

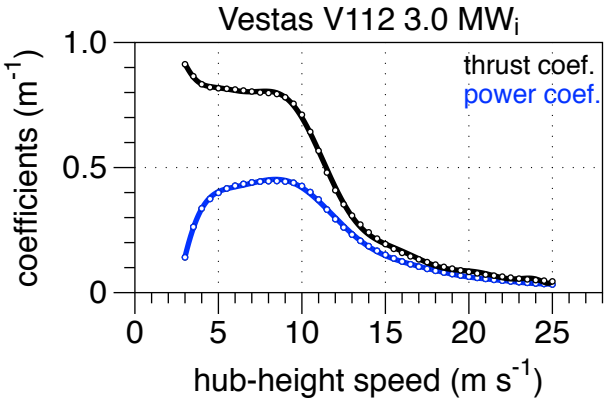

Figure 1: Shown as a function of the horizontal wind speed at the 84 meter hub-height, the manufacturer's data (points) for the thrust coefficient and derived power coefficient were included in this analysis as piece-wise polynomial fits (solid lines).

An initial model setup used the following physical parameterizations: WRF single-moment 6-class microphysics scheme (WSM6) [9]; Rapid Radiative Transfer Model longwave radiation scheme (RRTMG) [10], Goddard shortwave radiation scheme [5], Monin Obukhov surface layer physics [15], Mellor-Yamada-Janjic and Niino Level 2.5 (MYNN) for the planetary boundary layer [15], Betts-Miller-Janjic cumulus cloud scheme [11], and the Noah Land Surface Model for two-way land-atmosphere interactions [4]. Nudging was applied based on NCAR's WRF recommended values for grid resolutions of 10-30 kilometers, as a boundary width of 10 grid cells and a relaxation zone of 9 grid cells. Using a horizontal grid spacing of 12 km and 31 default vertical levels, we were able to reproduce the 10 meter wind speed dynamics of both the NARR forcing data and NCEP and ECMWF Reanalysis data (Fig. 2 & 3).

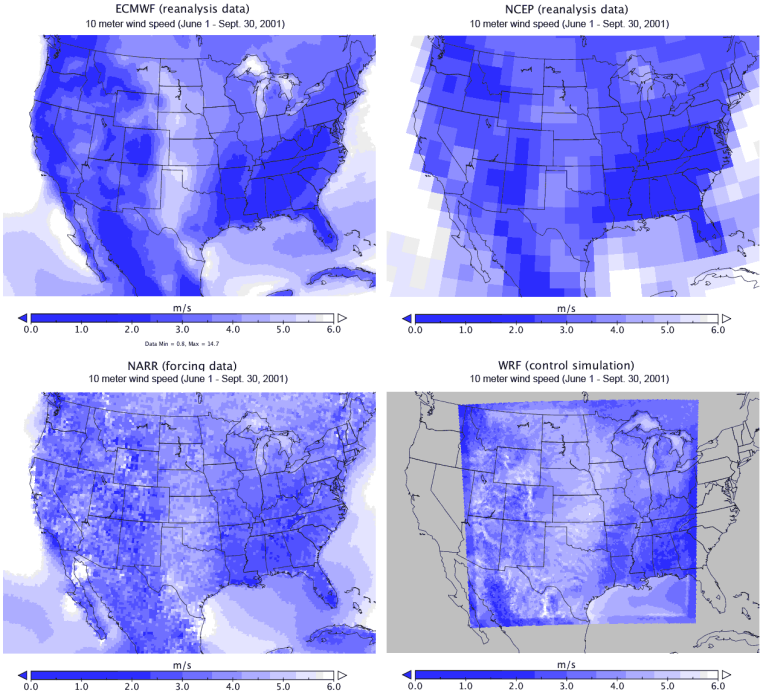

Figure 2: Mean 10 meter wind speed from June 1 - September 30, 2001. Note that in the lower right plot (WRF control simulation), the gray values reside outside the model domain.

To assess the sensitivity of this initial setup (*i.e.* 12 km horizontal grid resolution and 31 default vertical levels) to changes in the horizontal and vertical spacing, a series of additional model sensitivities were completed. Given our specific interest in wind power generation rates, we chose to focus these tests on a short time period: June 15-21, 2001, with June 15 excluded

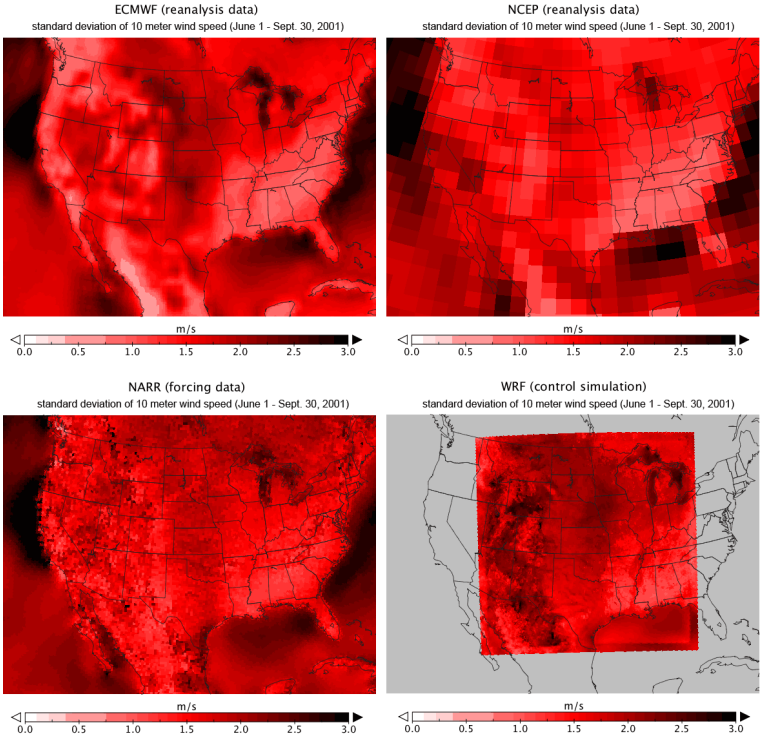

Figure 3: Standard deviation of 10 meter wind speed from June 1 - September 30, 2001. Note that in the lower right plot (WRF control simulation), the gray values reside outside the model domain.

from all analysis as spin up. As shown in Fig. 4, this time period covers the range of expected generation rates. For these tests though, only an installed capacity of 5 MW_i km^2 was simulated, as this is the commonly proposed large-scale installed capacity [12] and was thereby also the simulation most often to be compared to *VKE* of estimating wind power generation rates.

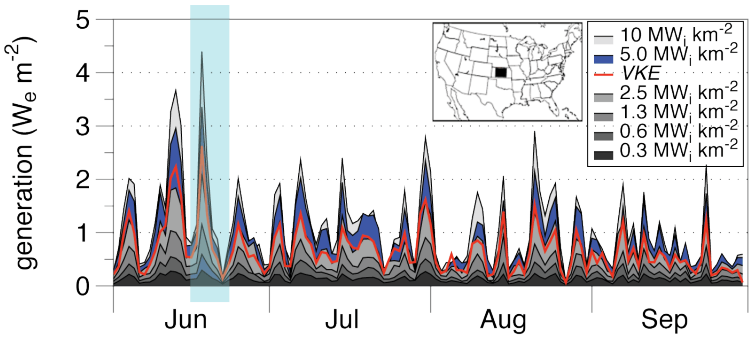

Figure 4: Showing the mean generation rates from June 1 - September 30, 2001 for the various installed capacities of 0.3125 - 100.0 MW_i km^2. The highlighted time period from June 16-21 shows the test time period for various horizontal and vertical spacing changes, as it corresponds to some of the highest and lowest generation rates for the 4-month period.

Overall, the results were quite comparable. Using a horizontal resolution of 12 km and 31 vertical levels resulted in a mean generation rate of 1.88 W_e m^{-2} (quartile 1, Q1 = 0.91 W_e m^{-2}, Q2 = 1.63 W_e m^{-2}, Q3 = 2.80 W_e m^{-2}). The bottom-height of each level below 1 km in meters above ground level is: 0, 56, 136, 241, 372, 537, 748, 998. Given the vertical extent from 28-140 meters above ground of the turbine rotor, this indicates that 3 model levels are directly influenced by the wind turbines. Two interior nests of 6 and 3 km were then included, while maintaining the same 31 vertical levels and the wind farm now being located within the 3 km nest. This setup did increase the mean generation rate by 0.04 W_e m^{-2} to 1.92 W_e m^{-2} (Q1 = 0.98 W_e m^{-2}, Q2 = 1.50, Q3 = 2.88 W_e m^{-2}). Using the same 6 and 3 km nests as above, this time, 61 *eta levels* were prescribed at: 1.0, 0.995, 0.9925, 0.99, 0.9875, 0.985, 0.9825, 0.98, 0.975, 0.97, 0.965, 0.96, 0.955, 0.95, 0.945, 0.94, 0.935, 0.93, 0.925, 0.92, 0.915, 0.905, 0.895, 0.885, etc. This setup results in the bottom height of the 24 levels below 1 km in meters above ground level as: 0, 40, 60, 80, 100, 120, 140, 161, 201, 242, 283, 324, 365, 406, 448, 490, 532, 574, 616, 658, 701, 786, 873, 960. With 6 vertical levels within the turbine rotor swept area and a horizontal resolution of 3 km, this model setup is approaching the resolutions of the original Fitch et al. [7], who completed their WRF simulations using 1 and 2 km horizontal spacing,

30 levels in the lowest 1 km, and 8 levels intersecting the rotor area. This 3 km horizontal high resolution vertical setup resulted in a mean generation rate of 1.74 W_e m^{-2} (Q1 = 0.80 W_e m^{-2}, Q2 = 1.40 W_e m^{-2}, Q3 = 2.77 W_e m^{-2}).

Given how closely the 12 km horizontal 31 default vertical level simulation compares with the setup almost consistent with the original wind power parameterization [7] testing, we chose to use the 12 km horizontal 31 default vertical level setup for all analysis in the main manuscript. Even given this similarities though, further study would be necessary to determine how well this parameterization setup reproduces operational wind farm data or hub-height wind velocities at 84 meters within this region of Kansas in 2001. While we strive to reproduce the typical climatic conditions occurring in this region during 2001 [17], the more critical focus of this study was to illustrate the dynamic of electricity generation rates when wind turbines are increasingly deployed into these typical climatic conditions. This model setup accomplishes that goal, while providing the opportunity for increased refinements in the future related to varied horizontal and vertical resolutions, wind turbine placement, and other time periods.

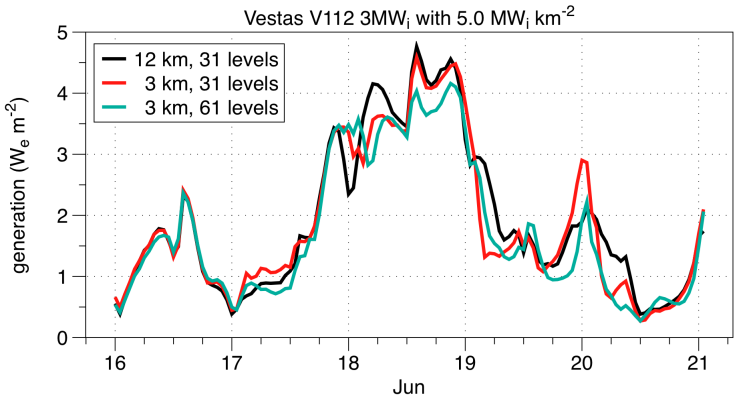

Figure 5: Showing the mean generation rates from June 16 - 21, 2001, with all simulations using an installed capacity within the Kansas wind farm region of 5.0 MW_i km^2.

3 Vertical Kinetic Energy Flux Method (*VKE*)

This method (*VKE*) extends the methodology in Gans et al. [8], allowing the maximum wind power potential to be estimated from the control climatological conditions before wind power is deployed. As three different methodologies were shown in [8] with additional similarities to the *simple momentum model* in [14], we will first review a general form and then show

how *VKE* can be applied to standard WRF 'pre-turbine' output data. Beginning with the general form, we define the steady-state momentum balance at hub-height (84 m) as:

$$\frac{dp_{hub}}{dt} = 0 = F_{transfer} - F_{surface} - F_{turbine} \tag{1}$$

where $F_{transfer}$ is the vertical momentum import rate from above, downward through the hub-height, $F_{surface}$ is the vertical transfer of momentum to the surface, and $F_{turbine}$ is the momentum transfer to the wind turbine, available due to the entrainment of upper-atmospheric momentum from above the atmospheric boundary layer. The momentum transfer to the surface is parameterized as:

$$F_{surface} = \rho C_{DN} \cdot v_{hub}^2 \tag{2}$$

where ρ is the air density at hub-height. The surface friction is defined as:

$$C_{DN} = k^2 \left(\ln \frac{z}{z_0} \right)^{-2} \tag{3}$$

Assuming a steady-state with $\frac{dp_{hub}}{dt} = 0$, the balance of momentum at hub-height can be expressed as:

$$0 = F_{transfer} - (\rho C_{DN} \cdot v_{hub}^2) - F_{turbine} \tag{4}$$

The kinetic energy withdrawn from the atmosphere by the wind turbine per unit surface area is:

$$P_{ex} = F_{turbine} \cdot v_{hub} \tag{5}$$

By combining Equations 4 and 5, the withdrawal rate from the instantaneous downward transport of kinetic energy through hub-height and thereby the maximum generation rate of the wind turbines can be maximized. This results in the new steady-state wind speed: $v_{hub} = \frac{\sqrt{3}}{3} v_0$, where v_0 is the hub-height wind speed of the control climatology before any wind turbines are installed. This corresponds to a decrease in wind speed at the maximum withdrawal rate by $1 - \frac{\sqrt{3}}{3} = 42\%$. The maximum withdrawal rate of kinetic energy from the atmosphere is then:

$$P_{max} = \frac{2\sqrt{3}}{9} F_{transfer} v_0 \tag{6}$$

This expression depends on the hub-height wind speed before the wind turbines are installed and the vertical momentum flux, $F_{transfer}$. It estimates the maximum rate by which atmospheric kinetic energy can be withdrawn, based on momentum conservation and the vertical momentum flux. Given that wind turbines unavoidably introduce turbulence in the turbine's wake during the withdrawal process [7], not all of the kinetic energy withdrawn from the atmosphere is converted to electricity. By assuming that

the present-day efficiency of a wind turbine can be approximated by the 59.3% Betz Limit [2], only about $\frac{2}{3}$ of the kinetic energy could be maximally converted to electricity (see [6]), resulting in:

$$P_e = \frac{4\sqrt{3}}{27} F_{transfer} \cdot v_0 \tag{7}$$

To illustrate the potentially surprising efficiency of present-day wind technology and how it compares to the theoretical Betz Limit of 59.3%, we compare the electricity generation rates for a single isolated turbine in Fig. 6. Defined as:

$$G_e = 0.593 \cdot (0.5\rho v^3) \cdot A_{rotor}/10^6 \tag{8}$$

where ρ is defined here as 1.1 kg m^{-3} and A_{rotor} is 9852 m^2, giving it the same rotor swept area as the Vestas V112. Note how the two curves diverge as the Vestas V112 power curve saturates about 11.5 m s^{-1}. This is a technological limitation that occurs with all wind technologies, and is not specific to the Vestas V112. *VKE* does not consider the technological limitations which cause the turbine power curves to saturate. This was done intentionally, making *VKE* independent from specific wind turbine specifications. Estimates resulting from *VKE* are also independent from a specified quantity of wind turbines deployed over a specific spatial area, where for example, high unit area (W_e m^{-2}) generation rates might only be possible during windy conditions if large quantities of wind turbines were present.

By deriving the generation rate from the natural climatic conditions without being tied to a specific turbine size, adequate spacing to match forcing conditions, or adequate quantities of such turbines to achieve maximum generation rates, the *VKE* quantifies the generation rates spatially and temporally while minimizing changes to the vertical transport of kinetic energy or the free atmospheric flow above the wind turbines. To summarize, this method includes limits to kinetic energy availability and extractability, but it does not enable the wind turbines to alter the control climatology, which as shown by the *WRF* simulations (*e.g.* Fig. 3 & 4) may locally increase generation rates.

The above notes the general form of *VKE* and its theoretical background, consistent with the methodology of Gans et al. [8]. In this study, to apply *VKE* to the *WRF* hourly output of the control simulation to estimate the maximum generation rate of electricity, we use:

$$P_e = \frac{4\sqrt{3}}{27} \cdot \rho u_*^2 \cdot v_0 \tag{9}$$

which uses the standard model output parameters of friction velocity (u_*), air density (ρ), and wind speed at hub height (v_0), with ρu_*^2 quantifying the momentum flux to the surface. The hub-height speed (v_0) is derived by post-processing the WRF output wind velocities per model layer and timestep to

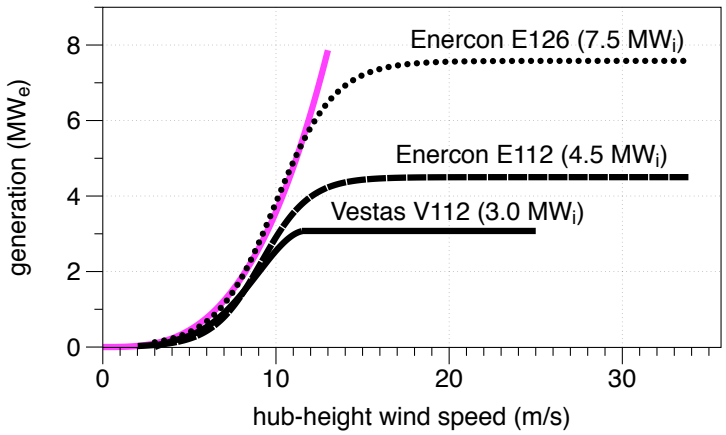

Figure 6: The black lines represent power curves for three different wind turbines, all based on an air density of 1.225 kg m^{-3}. For comparison purposes, the pink line uses a rotor area (A_{rotor}=9852 m^2) specific for the Vestas V112. For this cross-sectional area, this pink line represents the maximum single turbine extraction rate of kinetic energy theoretically possible.

84 meters using WRF's UPP v1.0 post processor and adding heights to the optional flight level specification. Note how the maximum generation rate of *VKE* therefore equivalent to $\frac{4\sqrt{3}}{27} = 26\%$ of the instantaneous downward transport of kinetic energy though hub-height or 26% of the dissipation occurring prior to wind turbine deployment, providing a means to compare other local- and large-scale estimates.

4 Supplemental tables and figures

	mean percent difference				
installed capacity (MW_i km^{-2})	10 m speed (% · 100)	84 m speed (% · 100)	nighttime ABLH (% · 100)	daytime ABLH (% · 100)	surface mom. flux (% · 100)
0.3125	-1.5	-5.0	+18.3	+0.8	-15.6
0.625	-1.1	-8.9	+33.6	+4.3	-15.6
1.25	-5.1	-15.5	+41.9	+1.7	-22.1
2.5	-10.2	-21.5	+57.3	+3.7	-30.4
5.0	-20.6	-30.8	+79.9	+4.3	-45.7
10.0	-33.5	-41.8	+151.7	+4.7	-61.2
25.0	-48.2	-54.6	+269.4	+5.6	-75.0
100.0	-59.2	-64.3	+349.7	+6.4	-84.4

Table 1: Based on simulations of *WRF*, relative climatic differences within the wind farm region compared to the control. ABLH is an abbreviation for atmospheric boundary layer height.

installed capacity (MW_i km^{-2})	number of turbines (#)	$\sum$ install capacity (GW_i)	electricity generation (GW_e)	elec. gen. per turbine (MW_e)	capacity factor (% · 100)	wind farm. elec. gen. (W_e m^{-2})
0.3125	11 700	35	14.8	1.27	42	0.13
0.625	23 400	70	27.3	1.17	39	0.24
1.25	46 800	140	46.3	0.99	33	0.41
2.5	93 600	281	76.0	0.81	27	0.68
5.0	187 200	562	106.5	0.57	19	0.95
10.0	374 400	1 123	124.0	0.33	12	1.10
25.0	936 000	2 808	114.0	0.12	4	1.02
100.0	3 744 000	11 232	65.8	0.02	0.6	0.59

Table 2: Based on simulations of the *WRF*, noting the relationship between the installed capacity and the electricity generation rates

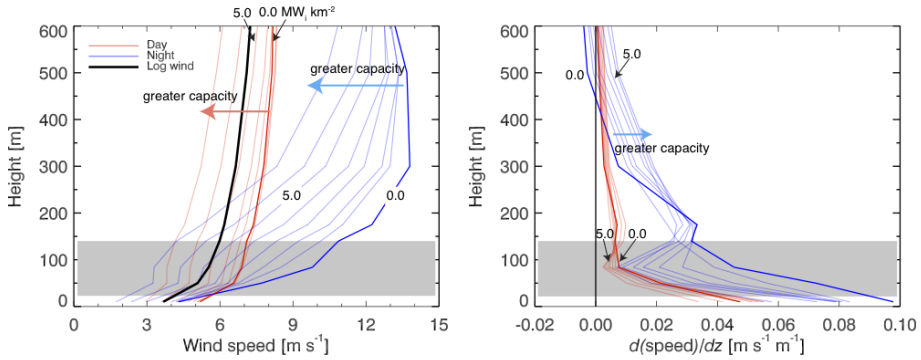

Figure 7: Using the *WRF* simulations, left: day (red) and night (blue) profiles of mean wind for the different installed capacities, with the data subset area shown in Figure 8. The thick red and blue lines represent the control simulation. The thick black line represents a simple log-wind profile derived from constant flux (stress), assuming $z_0 = 0.15$ m; $u_* = 0.35$ m s^{-1}. Right: profiles of the vertical derivative (gradient) of the wind speed, with line definitions as in the Left. In both, the shaded gray region represents the vertical rotor swept height.

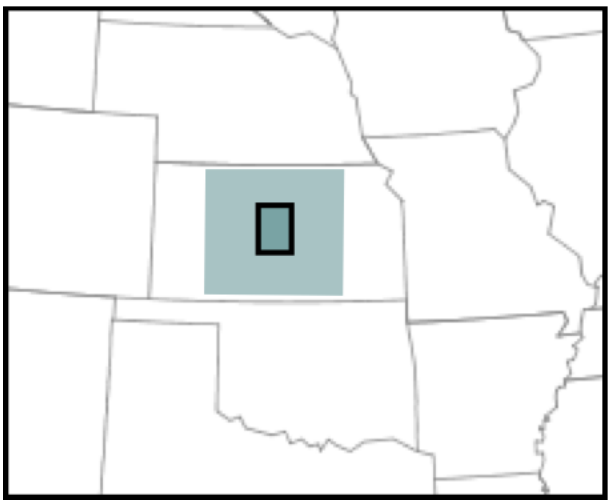

Figure 8: Showing the Kansas wind farm region (light shaded square), with the inset darker rectangle identifying the region used for quantifying the values in Fig. 7. Only the interior grid cells were analyzed to prevent the inclusion of edge effects.

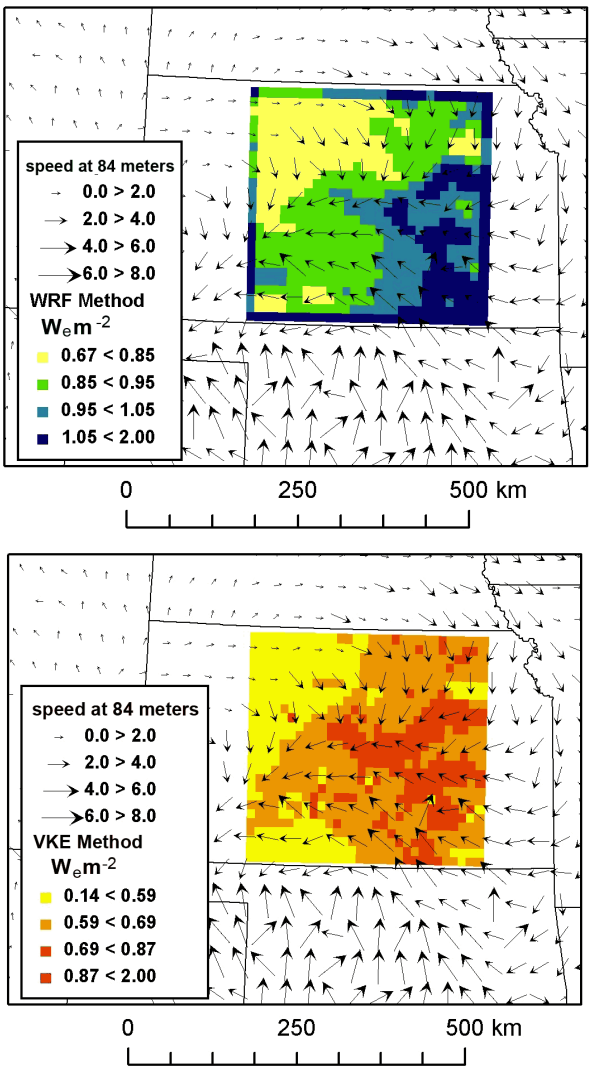

Figure 9: Mean electricity generation rates using *WRF* with an installed capacity of 5 MW_i km^{-2} (top), and (bottom) mean generation rates using *VKE*. Note the similar spatial structure, but prominent 'edge' of higher generation rates in *WRF*. This edge effect relates to horizontal transport of kinetic energy into the wind farm region (Section 5 of main text), which increases the generation rate of the wind turbines along the edge of the wind farm region. Breaks in the color bar differ, allowing for a better spatial comparison between the two estimates.

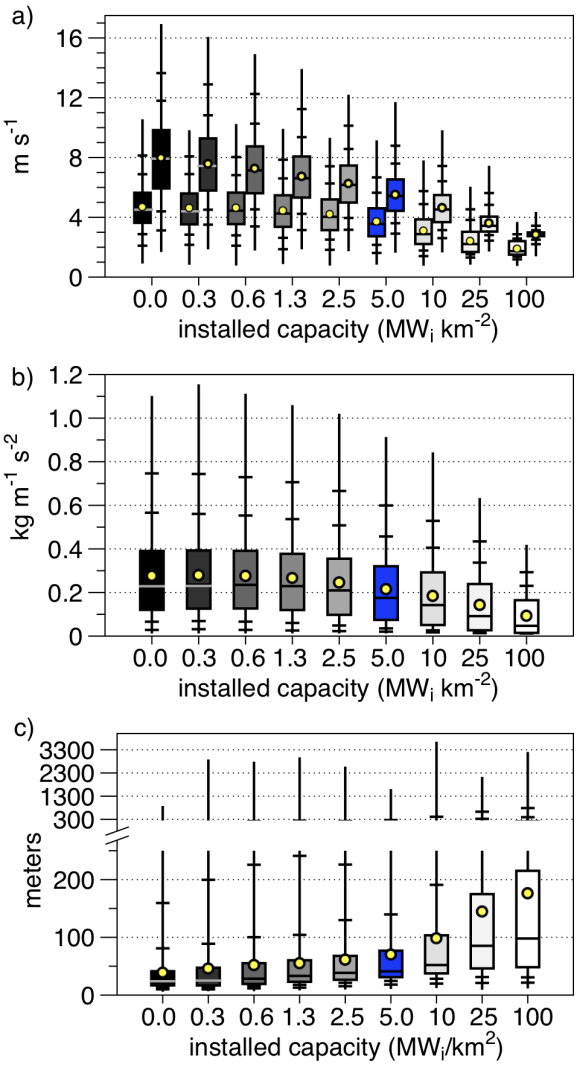

Figure 10: Quantified as the mean hourly value within the wind farm region for each of the simulations: **a)** 10 and 84 meter (hub-height) velocity, **b)** surface momentum fluxes (ρu_*^2), and **c)** nighttime boundary layer height. Mean values are shown as yellow circles; the extent of the vertical line is the min-max; the box represents the 1st quartile, median, and 3rd quartiles; the whiskers are at 2.5%, 10%, 90%, and 97.5%. Related percent differences are noted in Table 1.

References

[1] Adams A S and D Keith, (2013) Are global wind power resource estimates overstated? *Environ. Res. Lett.* 8, 015021

[2] Betz A, (1920) The maximum of theoretically available potential of wind by wind turbines (originally German). *Z. Gesamte Turbinenwesen*, Heft 26.

[3] Bukovsky M and D. Karoly, (2011) A Regional Modeling Study of Climate Change Impacts on Warm-Season Precipitation in the Central United States. *J. of Climate* 24, 1985-2002

[4] Chen F and J Dudhia, (2001) Coupling and advanced land surface-hydrology model with the Penn State-NCAR MM5 modeling system. Part I: model implementation and sensitivity. *Mon. Wea. Rev.* 129, 569-585

[5] Chou M and M Suarez (1999), A solar radiation parameterization for atmospheric studies. NASA Tech. Rep. NASA/TM-1999-10460, vol. 15, 38 pp

[6] Corten G, (2001) Novel Views on the Extraction of Energy from Wind-Heat Generation Concentration and Terrain, EWEC-CONFERENCE, 2001. 5p, downloaded on July 18, 2013 from http://www.ecn.nl/docs/library/report/2001/rx01054.pdf

[7] Fitch A, Olson J, Lundquist J, Dudhia J, Gupta A, and Michalakes J, (2012) Local and mesoscale impacts of wind farms as parameterized in a mesoscale NWP model. *Mon. Weather Rev.* 140, 3017-38

[8] Gans F, Miller L M, and Kleidon A. (2012) The problem of the second wind turbine — a note on common but flawed wind power estimation methods. *Earth Syst. Dynam.* 3, 79-86

[9] Hong SY and Lim JOJ. (2006)The WRF single-moment 6-class microphysics scheme (WSM6). *Journal of the Korean Meteorological Society*, 42, 2, 129-151

[10] Iacono M, Selamere J, Mlawer E, Shephard M, Clough S, and W Collins. (2008) *Journal of Geophysical Research*, 113, D13103

[11] Janjic Z. (1994) The step-mountain Eta coordinate model: Further developments of the convection, viscous sublayer, and turbulence closure schemes. *Mon. Wea. Rev.*,122, 927-945

[12] Lopez A, Roberts B, Heimiller D, Blair N, and Porro G, (2012), U.S. Renewable energy technical potentials: a GIS-based analysis, U.S. Department of Energy National Renewable Energy Laboratory NREL/TP-6A20-51946.

[13] Mesinger F, and coauthors, (2006), North American Regional Reanalysis. *Bull. Amer. Meteor. Soc.*, 87, 343-360

[14] Miller L M, Gans F, and Kleidon A, (2011), Estimating maximum global land surface wind power extractability and associated climatic consequences. *Earth Syst. Dynam* 2, 1-12

[15] Nakanishi, M. and H. Niino, (2009) Development of an improved turbulence closure model for the atmospheric boundary layer. *J. Meteor. Soc. Japan*, 87, 895-912

[16] Skamarock W C et al. (2008) A description of the advanced research WRF version 3 NCAR Technical Note NCAR/TN-475+STR

[17] Trier S., Davis C, and Ahijevych D (2010) Environmental controls on the simulated diurnal cycle of warm-season precipitation in the continental United States. *J. Atmos. Sci.*, 67, 1066-1090.